Electron transport process in quantum cascade intersubband semiconductor lasers

K. Kalna[a)]
Device Modelling Group, Department of Electronics and Electrical Engineering, University of Glasgow, Glasgow G12 8LT, Scotland, United Kingdom

C. Y. L. Cheung[b)] and K. A. Shore
School of Informatics, University of Wales, Bangor, Bangor LL57 1UT, Wales, United Kingdom

(Received 8 September 2000; accepted for publication 13 November 2000)

Detailed self-consistent calculations have been performed of the electron transport and capture aspects of the dynamics of electrically pumped quantum cascade intersubband semiconductor lasers. Specific attention is given to the dependence of the characteristic carrier relaxation times on carrier temperature and density at different applied biases. We have found that the capture and intersubband relaxation times oscillate with increasing electric field. Correlative oscillations can be observed when electron temperature and electron density is plotted as a function of the same applied bias at each energy subband of the laser active region. The temperature and density amplitude are rather less pronounced than those of the relaxations time. Analysis of this typical behavior suggests that the most effective laser structure should work under 70 meV bias. © *2001 American Institute of Physics.* [DOI: 10.1063/1.1339859]

I. INTRODUCTION

The present contribution reports calculations of the fundamental time constants which determine the dynamics of carrier transport and carrier capture in intersubband quantum cascade semiconductor lasers. Intersubband lasers (ISL) have become a topic of active research particularly following the development by Faist *et al.* of midinfrared quantum cascade lasers.[1] That work was the practical demonstration of a long standing proposal for the utilization of intersubband transitions to obtain lasing action in semiconductor superlattices.[2] Subsequent research at AT&T, Lucent,[3,4] and in a growing number of laboratories in the United States and Europe has given rise to significant developments in the performance of quantum cascade lasers. In this context it is of considerable interest to examine the dynamical behavior of quantum cascade lasers with a view, in particular,to evaluating the achievable direct current modulation characteristics of such lasers. It is noted that the picosecond carrier lifetimes which are characteristic of the operation of intersubband lasers may be anticipated to offer opportunities for tetrahertz (THz) bandwidth modulation in such lasers. This aspect has been previously examined where use was made of a rate equation model described in Refs. 5 and 6 to derive expressions for the modulation response of unipolar semiconductor lasers.[7] Subsequent work[8] has generalized that approach to yield a self-consistent rate equation analysis where, in particular, carrier lifetimes are deduced from calculations of electronic wave functions in the structure. That work indicated that modulation bandwidths of order 150 GHz would be obtainable in the chosen structure. In a recent brief report[9] it was indicated that unipolar lasers have the potential for achieving THz modulation bandwidths. All that work was concerned with the dynamical processes occurring in a single triple-quantum well element. In practical intersubband lasers, in order to achieve sufficient optical gain, the active region must contain many copies of such elements so as to achieve the quantum cascade effect which underpins the successful operation of this class of lasers. In order to analyze the dynamical processes at play in such a quantum cascade laser attention needs to be given to carrier transport and carrier capture processes which will affect, in particular, the achievable direct current modulation frequency of intersubband cascade lasers. In previous work[10] a theoretical framework was established to perform calculations of the pertinent physical factors which govern the carrier transport. Specific attention is given here to the determination of the dependence of the characteristic carrier relaxation times on carrier temperature and energy at different applied biases. These times have been calculated considering electrons emitting and absorbing polar optical and acoustic phonons and also effects of forward and backward transitions on final relaxation times have been examined. Finally, the Fermi exclusion principle has been taken into account in these calculations.

II. SELF-CONSISTENT ANALYSIS OF ELECTRON DYNAMICS

The generic structure which is assumed to form the building block of the active layer of the electrically pumped ISL of interest here has two main regions, an injection region and an active region as shown in Fig. 1. The injection region is fabricated by the eight quantum wells (QWs) capable of supplying electrons to the active region. The active region of the laser (see Fig. 1) is made up from a coupled triple quan-

a)Electronic mail: kalna@elec.gla.ac.uk
b)Present address: Motorola GSD, Blagrove, Swindon SN5 8YQ, Wales, United Kingdom.

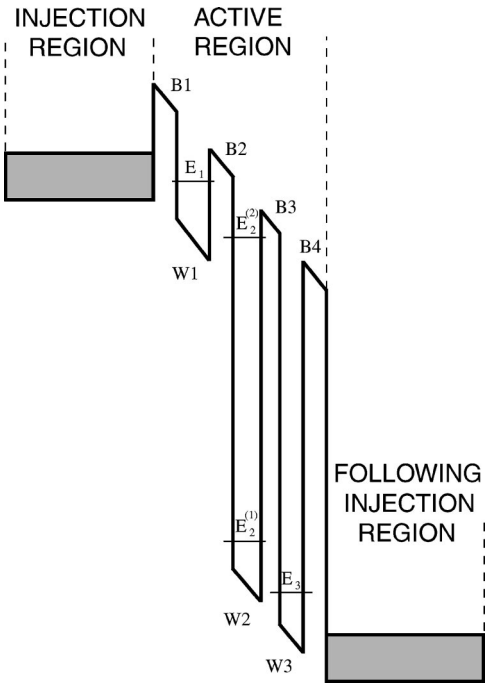

FIG. 1. Schematic diagram of the triple-quantum well cascade laser as considered in the self-consistent calculations. The active region consists of three quantum wells W1, W2, and W3 surrounded by barriers B1, B2, B3, and B4. Energy level E_1 is in the quantum well W1, levels $E_2^{(1)}$ and $E_2^{(2)}$ in W2, and level E_3 in W3.

tum well element with an injector well (W1), a central laser well (W2), and an extractor well (W3). In general, the carrier transport between the wells is characterized by a capture time, $\tau_{\rm cap}$, which includes transitions from all eight energy subbands in the injection region into all four energy subbands in the active region. Thus, this capture time already incorporates the tunneling time τ_{12} describing injection from quantum well W1 to quantum well W2—the lasing well and a tunneling time, τ_{23}, from the lasing well to quantum well W3, the extractor well as has been considered in previous work.[5–8] That work further assumed that the laser dynamics is determined by the carrier transit time through the structure, τ_T, and intersubband radiative relaxation time, τ_S. In the present work, we consider an intersubband relaxation time, $\tau_{\rm int}$, which incorporates transitions from the energy subbands E_1 (see Fig. 1) and $E_2^{(2)}$ into subbands $E_2^{(1)}$ and E_3. The essence of the present work is to perform quantum mechanical calculations of both the carrier relaxation times with a view to determining the dynamical properties of triple-quantum well cascade lasers (TQWCLs) under applied bias. Thus, the tunneling times are not treated as free parameters.

Our analysis is based on a structure which is designed for operation frequencies around 30 THz. These frequencies require a lasing wavelength of, nominally, 10 μm, so we shall apply a suitable bias voltage to the structure, such that the separation between the two energy levels involved in the transition is of this value. We have chosen a range of the bias from 60 to 80 meV. The lasing transition should have an energy from 117 meV under the lower applied bias of 60 meV up to 124 meV under the upper bias limit of 80 meV. We believe that the laser structure considered in this article can achieve the best performance within this range.

The methodology used is to undertake self-consistent calculations of the carrier times, carrier densities and temperatures, energy density, and optical gain appropriate to the ISL. Use is made of the argument principle method (APM) (described in Ref. 8) to perform calculations of the wave functions and carrier lifetimes for the relevant coupled quantum well structure. Those times are utilised in carrier rate equations[7] to obtain carrier densities in the appropriate energy subbands of the relevant structures. Such carrier densities can be used to calculate energy densities and carrier temperatures which are themselves taken to obtain the corresponding optical gain in the structure. That gain is then re-used in the carrier rate equations to calculate relevant capture and intersubband relaxation times and the whole process can be repeated. Iterations proceed until convergence is obtained. For the cases studied here that convergence is, in fact, quite rapid and only around ten iterations are required. Several aspects of the procedure have been described in earlier works[7–9] and, hence, it is not appropriate to rehearse those elements here.

Electron relaxation dynamics in the ISL are governed predominantly by the electron interaction with polar optical phonons. Nevertheless, in order to verify its contribution we have also taken into account, via the deformation potential interaction, electron scattering by acoustic phonons. Both phonons are considered to be bulk-like because incorporation of some phonon confined model affects the overall results to a degree ($<5\%$) comparable to other fine effects such as nonparabolicity.[11] The electron-phonon rates are calculated using Fermi's golden rule as a transition from the initial subband i with energy E_i to the final subband j with energy E_j. Then the electron rate with an initial energy E can be obtained for the polar optical phonon (POP) scattering as[12–14]

$$\Gamma_{ij}^{\rm PO\pm}(E)=\frac{e^2\omega_{\rm PO}m}{8\pi\hbar^2}\left(\frac{1}{\kappa_\infty}-\frac{1}{\kappa}\right)\int_0^{2\pi}d\theta\left(N_{\mathbf{q}}+\frac{1}{2}\pm\frac{1}{2}\right)\times\frac{F_{iijj}(q)}{q}, \tag{1}$$

where the POP wave vector is

$$q=\frac{\sqrt{2m}}{\hbar}[2E-E_{\rm PO}-2\sqrt{E(E+E_{\rm PO})}\cos\theta]^{1/2}, \tag{2}$$

with $E_{\rm PO}=E_i-E_j\mp\hbar\omega_{\rm PO}$. In the earlier formulas (1) and (2) and in each formula which follows, the upper sign stands for the phonon emission while the lower one for the phonon absorption, $\omega_{\rm PO}$ is the POP frequency, m is the electron effective mass, κ_∞ and κ are the high-frequency and static permittivities, respectively. The phonon distribution function $N_{\mathbf{q}}$ is the Bose distribution. The phonon frequency ω in the case of polar optical phonons is dispersionless ($\omega=\omega_{\rm PO}$). The form factor, F_{iijj},[10] is calculated using the wave functions obtained using the APM method.[8] The screening of the electron-phonon interaction can be neglected for electron densities less than 10^{14} m^{-2} at room temperature.[15]

The relaxation rate of an electron with initial energy E scattered by an acoustic phonon (AP) reads

$$\Gamma_{ij}^{\mathrm{AC}\pm}=\frac{D^2 m}{8\pi\hbar^2\rho v_S}\int_0^{2\pi} d\theta \left(N_{\mathbf{q}}+\frac{1}{2}\pm\frac{1}{2}\right) q^2 F_{iijj}(q), \quad (3)$$

where the AP wave vector is

$$q=\frac{\sqrt{2m}}{\hbar}[2E-E_{\mathrm{AC}}-2\sqrt{E(E+E_{\mathrm{AC}})}\cos\theta]^{1/2}, \quad (4)$$

with the elastic equipartition approximation given by $E_{\mathrm{AC}}=E_i-E_j$.[13] Because the lattice temperatures T_L in our ISL are sufficiently high and any electron with a very high kinetic energy is quickly thermalized by the intrasubband electron–electron (e–e) interaction, the equipartition approximation works very well.

In formulas (3) and (4) for the electron rate, D is the acoustic deformation potential, ρ is the mass density, and v_S is velocity of sound in the material. The phonon frequency ω in the case of APs can be approximated by the linear dispersion relation as $\omega=v_S q$.[13]

The capture and intersubband relaxation times are sums of the averaged electron intersubband rates

$$\frac{1}{\tau}=\sum_i \frac{1}{n_{Si}}\sum_j \int_0^{\infty} dE\{f_i(E)[1-f_j(E')][\Gamma_{ij}^{+}(E) + \Gamma_{ij}^{-}(E)]-[1-f_i(E')]f_j(E)[\Gamma_{ji}^{-}(E)+\Gamma_{ji}^{+}(E)]\}, \quad (5)$$

where

$$\Gamma_{ij}^{\pm}=\Gamma_{ij}^{\mathrm{PO}\pm}+\Gamma_{ij}^{\mathrm{AC}\pm}, \quad (6)$$

n_{Si} represents the sheet electron density in the ith subband, and the electron final energy $E'=E\mp E_{\mathrm{PO}}$ or $E'=E\mp E_{\mathrm{AC}}$, respectively. The electron distribution functions f_i and f_j are taken as Fermi distributions whose quasi-Fermi energy is a function of the electron temperature and the sheet electron density which are obtained from rate equations.[7]

Since typical electron densities in the TQWCL are less then 10^{14} m^{-2} we can safely neglect any contribution of intersubband e–e interactions to the capture and intersubband relaxation times. With the exception of oscillation resonances, the e–e capture time is two to three orders of magnitude larger than the electron-phonon capture time.[15] The effect of the e–e interaction on the overall capture time is even further suppressed when the exchange effect is taken in to account.[16] Note that inclusion of the degeneracy has no impact on the e–e capture time for actual electron densities in the laser ($<10^{14}$ m^{-2}).[16] Similarly, the e–e interaction can be omitted when the intersubband relaxation time is calculated at room temperature. The intersubband e–e scattering rate in the GaAs QW is slower by several orders of magnitude than the intrasubband e–e scattering rate.[14]

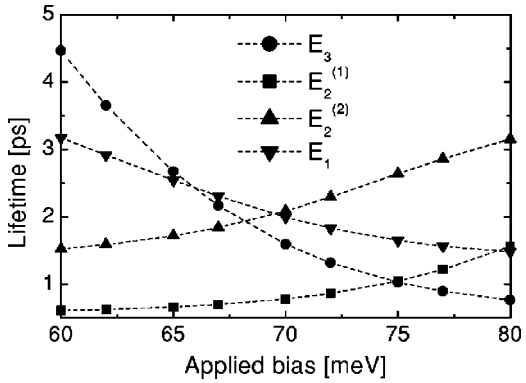

FIG. 2. State lifetimes vs applied bias at each energy subband of the active region.

III. STATE LIFETIMES

The time during which electrons remain trapped inside the active region of the TQWCL at a given subband energy is known as the state lifetime. This lifetime determines the fastest possible time response of a device and may be used to ensure that tunneling between the QWs is sufficiently fast so it is not affected by the inelastic scattering phenomena. Nevertheless, we do not rely upon any eventual limit set by the lifetimes because our calculations of the capture and intersubband relaxation times already include the tunneling phenomena through the form factor F_{iijj}.

The electron state lifetime is defined as $\tau=\hbar/\Gamma$, where Γ is the full width at half maximum of the Lorentzian resonance. It is obtained from the imaginary part of the complex energy eigenvalues from the numerical solution of the Schrödinger equation in the complex energy plane. The real part of the complex solution corresponds to the eigenenergy and the imaginary part is $\Gamma/2$. A direct relation can be observed in most cases, the higher the energy level, the shorter the corresponding state lifetime. The state lifetimes of bound states are infinite, while those of quasibound states are usually of the order of picoseconds or femtoseconds. However, in QW structures an inversion of lifetimes corresponding to their energy subbands can happen[17] as is the case with the TQWCL.[8]

Figure 2 shows electron state lifetimes at each energy subband which appears in the active region of TQWCL under chosen applied biases. The state lifetime of an electron at the subband E_3 (belonging to the last QW) is dropping sharply. This means that electron can be more rapidly depleted from the active region when the bias increases. Fortunately, the lifetime in subband $E_2^{(1)}$ (the lower one in the middle QW) increases relatively slowly compared with all other lifetimes. On the other hand, the lifetime in subband $E_2^{(2)}$ (the upper one in the middle QW) is increasing much more and therefore conditions for the creation of an inversion population become less favorable with increasing bias. The lifetime of the energy subband E_1 becomes still shorter under higher bias which should help to supply electrons for the creation of population inversion. Overall insight into the behavior of the lifetimes at all four subbands indicates that the best performance could be achieved under the lower bias. We will see in the following section that this rather straightforward conclusion have to be balanced with other TQWCL parameters.

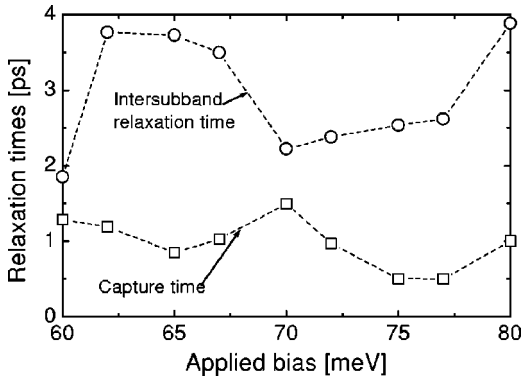

FIG. 3. Capture time and intersubband relaxation time vs applied bias in the TQWCL as obtained after the self-consistent calculations.

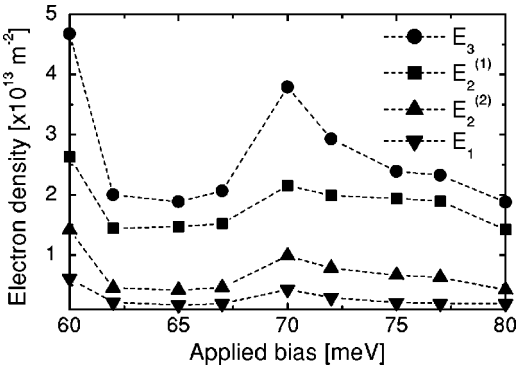

FIG. 4. Electron density vs applied bias at each energy subband of the active region.

IV. ELECTRON DYNAMICS UNDER APPLIED BIASES

Relaxation times of interest, the capture time and the intersubband relaxation time, are plotted as a function of the applied bias in Fig. 3. These relaxation times have been calculated as sums over initial states i and over final states j in Eq. (5). In a case of the capture time τ_{cap}, the sum over i involves all subbands in the injection region. The sum over j involves all four subbands in the active region. In the case of the intersubband relaxation time, τ_{cap}, the first sum goes over all upper subbands and the second one over all lower subbands in the active region only. We have found that the forward and backward processes are finely balanced when summing up contributions for a particular transition for the capture time. Even the backward processes are very effective for transitions from the lowest initial subband in the injection region (they are stronger by several order of magnitude); the importance of the forward process quickly increases and, in the final result, the contributions of these processes overcome the backward ones. Therefore, the whole electron capture process from the injection region into the active region is very effective.

On the other hand, the behavior of individual transitions for the intersubband relaxation time is much more forthright. Both the forward processes (emission and absorption) are two to three order of magnitude larger than the backward processes for each initial subband in the active region. Both times oscillate with increasing electric field due to actual difference between the energy subbands of initial and final states involved in the electron transitions. This can be understood in the same way as oscillations of the capture time versus QW width predicted in Ref. 18. The actual position of the energy subbands in the injection and active regions is changed in the TQWCL under increasing bias. An electron interaction with POPs is the main scattering process for each relaxation time. We have evaluated the particular importance of the electron interaction with both POP and AP. We have found that in the TQWCL the electron-POP rate is always about two orders of magnitude larger than the electron-AP rate for both capture and intersubband relaxation times which is a well-known electron transport characteristic in two-dimensional semiconductor heterostructures.[19] The efficiency of a particular electron transition depends on whether the energy difference between the initial and final energy levels is comparable to or greater than the POP energy.[15] In that case, an electron from the initial energy subband can undergo a very effective transition into the final subband even an interaction with acoustic phonons can work against it. We can see that the shortest capture and intersubband relaxation times occur at the bias of 70 meV. We can conclude that the efficiency of the TQWCL is optimized at this bias.

The same oscillations can be seen in Fig. 4 where the electron density, again as a function of applied bias, is shown at each energy subband in the active region. All four electron densities line up according to the energy level, the highest density is always at the lowest energy subband E_3, the density at the subband $E_2^{(1)}$ is always below the density at the subband E_3, and so on. The rapid increase of the electron densities at 70 meV bias causes both relaxation times to be short (see Fig. 3).

Finally, electron temperatures at each subband in the active region are plotted in Fig. 5 as a function of electric field. Temperatures at the subbands $E_2^{(2)}$ and E_1 are always about 10° higher than temperatures at the two lower subbands $E_2^{(1)}$ and E_3. The electrons at the two higher subbands lose sufficient energy by emitting photons when they fall down into the subbands $E_2^{(1)}$ and E_3 in the active region. The interesting fact is that while the electron temperature at the subband $E_2^{(2)}$ is practically constant under applied bias the electron temperature at the subband E_1 oscillates with quite large amplitude. This indicates that the most electrons emitting a photon come from the subband $E_2^{(1)}$ as expected.

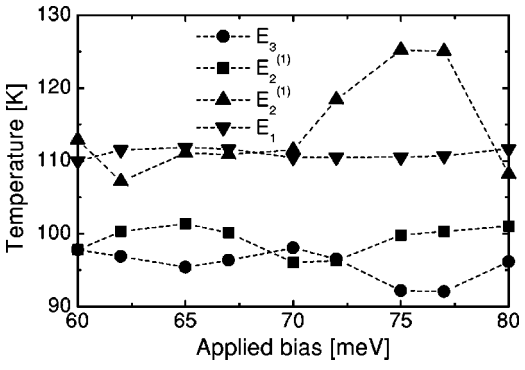

FIG. 5. Electron temperature vs applied bias at the same energy subbands.

V. CONCLUSION

We have performed self-consistent calculations of the capture and intersubband relaxation times in a loop with electron density and temperature at each energy subband of the proposed TQWCL structure. The whole process takes typically about ten iterations so convergence is quite fast. We have found that all calculated quantities (both relaxation times, electron densities, and temperatures) oscillate as a function of the applied bias. On the contrary, the state lifetimes at each subband of the active region increase (subbands $E_2^{(1)}$ and $E_2^{(2)}$) or decrease (subbands E_1 and E_3) smoothly under the bias and a crossover of the curves can be observed. When comparing a behavior of the both relaxation times, electron densities, and temperatures at each subband, the most effectively working TQWCL structure has been identified to be around 70 meV bias.

ACKNOWLEDGMENTS

K.K. appreciates a support from Royal Society for his visit to University of Wales, Bangor. EPSRC support is gratefully acknowledged by K.A.S.

[1] J. Faist, F. Capasso, D. L. Sivco, C. Sirtori, A. L. Hutchinson, and A. Y. Cho, Science **264**, 553 (1994).
[2] R. F. Kazarinov and R. A. Suris, Sov. Phys. Semicond. **5**, 797 (1971).
[3] J. Faist, F. Capasso, C. Sirtori, D. L. Sivco, A. L. Hutchinson, and A. Y. Cho, Appl. Phys. Lett. **67**, 3057 (1995).
[4] C. Sirtori, J. Faist, F. Capasso, D. L. Sivco, A. L. Hutchinson, and A. Y. Cho, IEEE Photonics Technol. Lett. **9**, 294 (1997).
[5] W. M. Yee, K. A. Shore, and E. Schöll, Appl. Phys. Lett. **63**, 1089 (1993).
[6] W. M. Yee and K. A. Shore, Semicond. Sci. Technol. **9**, 1190 (1994).
[7] C. Y. L. Cheung, P. S. Spencer, and K. A. Shore, IEE Proc.-J: Optoelectron. **144**, 44 (1997).
[8] C. Y. L. Cheung and K. A. Shore, J. Mod. Opt. **45**, 1219 (1998).
[9] N. Mustafa, L. Pesquera, C. Y. L. Cheung, and K. A. Shore, IEEE Photonics Technol. Lett. **11**, 527 (1999).
[10] K. Kalna, C. Y. L. Cheung, I. Pierce, and K. A. Shore, IEEE Trans. Microwave Theory Tech. **48**, 639 (2000).
[11] D. F. Nelson, R. C. Miller, and D. A. Kleinman, Phys. Rev. B **35**, 7770 (1987).
[12] P. J. Price, Ann. Phys. (N.Y.) **133**, 217 (1981).
[13] B. K. Ridley, J. Phys. C **15**, 5899 (1982).
[14] S. M. Goodnick and P. Lugli, in *Hot Carriers in Semiconductor Nanostructures*, edited by J. Shah (Academic, New York, 1992), p. 191.
[15] K. Kalna, M. Moško, and F. M. Peeters, Appl. Phys. Lett. **68**, 117 (1996).
[16] K. Kalna and M. Moško, Phys. Rev. B **54**, 17730 (1996).
[17] G. N. Henderson, L. C. West, T. K. Gaylord, C. W. Roberts, E. N. Glytis, and M. T. Asom, Appl. Phys. Lett. **62**, 1432 (1993).
[18] J. A. Brum and G. Bastard, Phys. Rev. B **33**, 1420 (1986).
[19] G. Bastard, *Wave Mechanics Applied to Semiconductor Heterostructures* (Les Editions de Physique, Les Ulis, France, 1998).